

Attention Illuminates LLM Reasoning: The Preplan-and-Anchor Rhythm Enables Fine-Grained Policy Optimization

Yang Li¹², Zhichen Dong¹², Yuhan Sun¹, Weixun Wang², Shaopan Xiong², Yijia Luo², Jiashun Liu², Han Lu¹², Jiamang Wang², Wenbo Su^{2*}, Bo Zheng², Junchi Yan^{1*}

¹Shanghai Jiao Tong University ²Alibaba Group

Abstract

The reasoning pattern of Large language models (LLMs) remains opaque, and Reinforcement learning (RL) typically applies uniform credit across an entire generation, blurring the distinction between pivotal and routine steps. **This work positions attention as a privileged substrate that renders the internal logic of LLMs legible, not merely as a byproduct of computation, but as a mechanistic blueprint of reasoning itself.** We first distinguish attention heads between locally and globally focused information processing and reveal that locally focused heads produce a sawtooth pattern near the diagonal indicating phrasal chunks, while globally focused heads expose tokens that exert broad downstream influence over future tokens. We formalize these with two metrics: 1) Windowed Average Attention Distance, which measures the extent of backward attention within a clipped window; 2) Future Attention Influence, which quantifies a token’s global importance as the average attention it receives from subsequent tokens. Taken together, these signals reveal a recurring preplan-and-anchor mechanism, where the model first performs a long-range contextual reference to generate an introductory token, which is immediately followed by or coincides with a semantic anchor token that organizes subsequent reasoning. Leveraging these insights, we introduce three novel RL strategies that dynamically perform targeted credit assignment to critical nodes (preplan tokens, anchor tokens, and their temporal coupling) and show consistent performance gains across various reasoning tasks. **By aligning optimization with the model’s intrinsic reasoning rhythm, we aim to transform opaque optimization into an actionable structure-aware process, hoping to offer a potential step toward more transparent and effective optimization of LLM reasoning.**

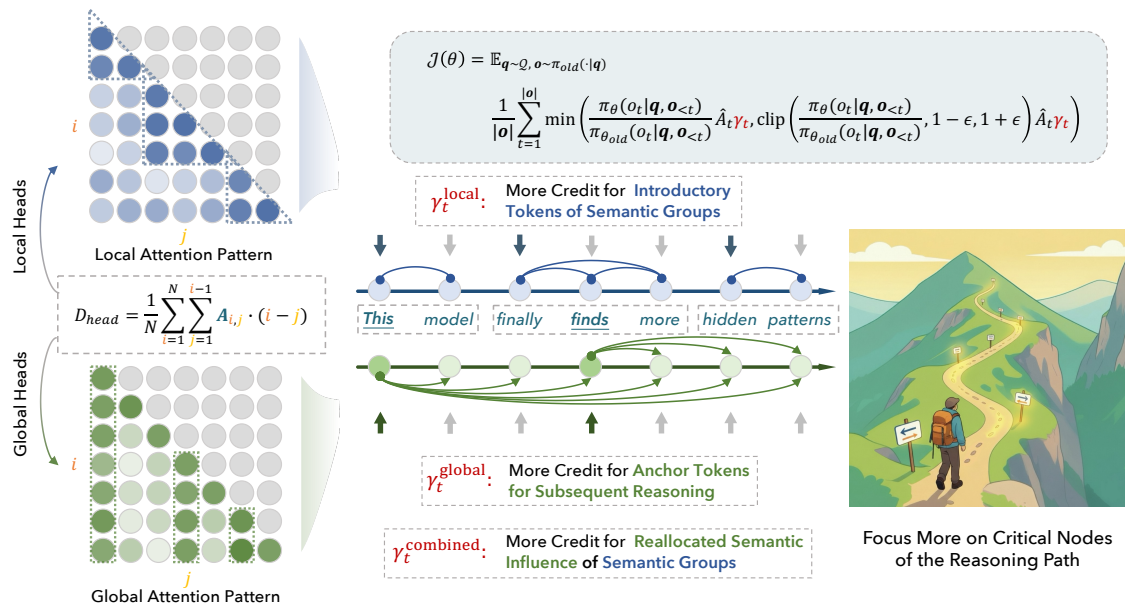


Figure 1: **Attention dynamics uncover reasoning patterns:** Local heads exhibit a near-diagonal, sawtooth pattern that forms phrasal chunks, while global heads highlight tokens with strong downstream influence. Their coupling reveals a preplan-and-anchor rhythm: at chunk onsets, preplan tokens set up the next reasoning step, followed (or coinciding) by anchor tokens that are persistently revisited by future tokens to guide downstream reasoning. **Reasoning rhythm enhances RL:** Leveraging detected preplan and anchor tokens, our RL method amplifies their token-level credit accordingly, focusing learning on the critical nodes that drive more effective reasoning.

*Correspondence authors. Junchi Yan: yanjunchi@sjtu.edu.cn; Wenbo Su: vincent.swb@taobao.com

1 Introduction

Large Language Models (LLMs) have achieved remarkable success on complex reasoning, propelled by training algorithms that elicit explicit step-by-step thought. A prominent paradigm is Reinforcement Learning with Verifiable Rewards (RLVR) (Lambert et al., 2024), where a model’s outputs are optimized with RL objectives guided by automated correctness checks. This setup encourages models to produce intermediate reasoning tokens before issuing a final answer, giving rise to Large Reasoning Models (LRMs) that excel on challenging problems in mathematics (Hendrycks et al., 2021; Cobbe et al., 2021b; Shao et al., 2024; Yang et al., 2024), coding (Chen et al., 2021; Jimenez et al., 2023; Hui et al., 2024), and agentic decision making (Liu et al., 2023; Yao et al., 2024).

Despite impressive performance, LLMs remain largely opaque: there still lacks a clear understanding of how LLMs structure their reasoning process internally, when and how they retrieve and bind information. Consequently, optimization strategies often treat an entire generation as a uniform target. In the popular RL settings, sequence-level rewards are typically spread across all tokens (Shao et al., 2024; Yu et al., 2025), blurring the distinction between pivotal moments that shape downstream reasoning and routine steps that merely elaborate local structure. This mismatch between how models appear to reason and how we optimize them limits data efficiency, interpretability, and the reliability of performance gains on challenging reasoning tasks. This paper seeks to bridge this gap by first showing an intrinsic reasoning rhythm through the lens of attention dynamics and subsequently introducing fine-grained RL strategies that enhance credit assignment to the tokens where the model appears to plan and anchor its reasoning.

Our analysis takes two complementary views of attention: a local (backward) perspective that measures how strongly a token depends on nearby versus distant context, and a global (forward) perspective that measures a token’s downstream influence on subsequent tokens. Specifically, we classify attention heads as either locally or globally focused based on their average attention span, which we define as the attention-weighted mean positional distance of their attention connections. Aggregating patterns within each class reveals two robust regularities as shown in Fig. 1. First, locally focused heads exhibit a sawtooth motif near the diagonal that tracks phrasal or semantic chunks. Within a chunk (e.g., habitual expressions), attention stays highly localized, while the onset of a new chunk pulls attention back to earlier context. Second, globally focused heads highlight a small set of anchor tokens that exert broad downstream influence. These tokens are revisited by many subsequent positions and act as semantic pivots that steer the unfolding reasoning.

We distill these regularities into two model-internal metrics computed from the attention map of an auxiliary forward pass. The **Windowed Average Attention Distance (WAAD, Def. 4.1)** measures how far a token looks back within a clipped window, emphasizing whether the model must reach beyond immediate neighbors to resolve ambiguity. Visualizing the WAAD sequence reveals a clear alternation between peaks and valleys, aligned with chunk boundaries. The **Future Attention Influence (FAI, Def. 4.1)** quantifies a token’s global importance by measuring the average attention it receives from later tokens. Visualizing the FAI sequence reveals differences and fluctuations in token influence, where high-influence tokens essentially correspond to key logical waypoints, such as pivotal definitions, intermediate results, or decision points. **The joint dynamics of the metrics** reveal a consistent two-beat preplan-and-anchor pattern. As the model approaches a semantic boundary, WAAD spikes as it consults longer-range context to draft an introductory token. This spike is often followed by, or coincides with, the emission of an anchor token with high FAI that organizes downstream inference. Additionally, WAAD spikes typically maintain high token entropies. The model reaches further back when nearby cues are insufficient to disambiguate the next step (e.g., when the preceding words do not naturally license the next token). Conversely, locally dominated tokens tend to have lower entropy, reflecting stereotyped continuations.

Building on the insights, we propose fine-grained policy optimization strategies that align credit assignment with the model’s intrinsic reasoning patterns. Rather than applying uniform advantages across a trajectory, we offer a process-aware alternative by leveraging internal, attention-based signals to differentially reinforce the steps the model itself treats as structurally decisive, as shown in Fig. 1: (1) emphasizing introductory tokens at chunk onsets (WAAD peaks) to establish the local scaffold for subsequent steps; (2) amplifying anchor tokens (high FAI) to articulate and preserve core semantic commitments that organize downstream inference, accelerating the propagation of verifiable signals to key decision points; and (3) when an anchor is locally dominated, reallocate part of its credit to the associated introductory token, promoting coherent chunk-level credit assignment rather than overfitting a single position.

Our contributions include: (1) We introduce attention dynamics as a principled lens for uncovering intrinsic reasoning structure in LLMs and empirically reveal the so-called preplan-and-anchor rhythm. We formalize this pattern through two novel metrics and analyze their joint behavior to characterize local phrasal processing and global contextual anchoring. (2) Building on these insights, we introduce three structure-aware reinforcement learning strategies that dynamically reweight token-level advantages to emphasize critical reasoning nodes, specifically, introductory preplan tokens, semantic anchor tokens and

their temporal coupling. (3) We demonstrate consistent and significant empirical gains across various reasoning benchmarks, validating our effectiveness and efficiency while maintaining compatibility with existing RLVR workflows.

2 Related Work

Reinforcement Learning for LLMs. Reinforcement learning (RL) is central to LLM post-training, popularized by RLHF for instruction following and preference alignment (Christiano et al., 2017; Ziegler et al., 2019; Ouyang et al., 2022; Schulman et al., 2022; Bai et al., 2022a). Two strands dominate: online policy-gradient methods with on-policy rollouts (Schulman et al., 2017; Shao et al., 2024; Williams, 1992) and offline preference optimization without on-policy sampling (Rafailov et al., 2023; Meng et al., 2024; Ethayarajh et al., 2024). Reinforcement Learning from AI Feedback (RLAIF) extends this by using LLMs to generate feedback for alignment (Bai et al., 2022b; Sun et al., 2023; Lee et al., 2023; Guo et al., 2024). Outcome-based **RL with verifiable rewards (RLVR)** (Shao et al., 2024; Lambert et al., 2025) has driven recent advances through deterministic rule-based rewards (Xin et al., 2024; Wang et al., 2024), with large-scale systems demonstrating that correctness-guided RL elicits extended reasoning (Lambert et al., 2024; OpenAI, 2024; Guo et al., 2025; Team et al., 2025; Yang et al., 2025a). A growing ecosystem studies data aggregation, policy updates, and scalable training infrastructure (Yu et al., 2025; Yue et al., 2025; Zheng et al., 2025; Liu et al., 2025).

Analyses of LLM Reasoning. A complementary literature analyzes how LLMs represent and execute reasoning (Wang et al., 2023; Ma et al., 2023; Dong et al., 2025; Yang et al., 2025b). Step-level edits suggest surface CoT redundancy (Wang et al., 2022; Madaan & Yazdanbakhsh, 2022; Wang & Zhou, 2024; Chen et al., 2024; Han et al., 2025; Wolf et al., 2025). White-box studies identify components that propagate information, such as iteration and receiver heads (Cabannes et al., 2024; Ren et al., 2024; Bertolazzi et al., 2025), critical subsets of attention heads (Geva et al., 2023; Mohebbi et al., 2023; Zheng et al., 2024), steerable planning/backtracking directions (Venhoff et al., 2025; Turner et al., 2024), and deduction circuits (Dutta et al., 2024; Ameisen et al., 2025; Lindsey et al., 2025). Additional phenomena include attention sinks on initial tokens (Xiao et al., 2023; Gu et al., 2025; OpenAI et al., 2025; Barbero et al., 2025) and anchor sentences that guide downstream inference (Bogdan et al., 2025; Men et al., 2024). These accounts, however, are often descriptive and rarely yield process-aware training recipes.

Within RLVR, analyses indicate that gains are driven by the emergence and macro-structure of explicit reasoning rather than answer correctness and the micro-content (Gandhi et al., 2025; Li et al., 2025). Other work targets critical tokens as decision points for exploration (Vassoyan et al., 2025; Lin et al., 2024) and emphasizes high-entropy *forking* tokens that govern divergent paths (Wang et al., 2025b;a; Cheng et al., 2025; Cui et al., 2025). Our approach differs by deriving model-internal signals from attention dynamics. We identify a recurring preplan-and-anchor rhythm, link key metrics to model-internal signals, and use these signals to perform targeted credit assignment within standard RL frameworks.

3 Preliminaries

3.1 Self-Attention Mechanism in Decoder-Only LLMs

Given the sampled question $\mathbf{q} \sim Q$, a decoder-only LLM policy π_θ autoregressively generates an output sequence \mathbf{o} , with \mathbf{o}_t as the t -th token in \mathbf{o} :

$$p_\theta(\mathbf{o} | \mathbf{q}) = \prod_{t=1}^T p_\theta(o_t | \mathbf{q}, \mathbf{o}_{<t}). \quad (1)$$

Within each Transformer layer l and head $h \in \{1, \dots, H\}$, multi-head self-attention computes head-specific attention maps:

$$\mathbf{S}^{(l,h)} = \frac{\mathbf{Q}^{(l,h)} \mathbf{K}^{(l,h)\top}}{\sqrt{d_k}} + \mathbf{M}, \quad \mathbf{A}^{(l,h)} = \text{softmax}(\mathbf{S}^{(l,h)}), \quad \mathbf{O}^{(l,h)} = \mathbf{A}^{(l,h)} \mathbf{V}^{(l,h)}, \quad (2)$$

and aggregates heads via $\text{MHA}(\mathbf{X}) = [\text{Concat}_{h=1}^H \mathbf{O}^{(l,h)}] \mathbf{W}_O^{(l)}$. Causal masking enforces autoregressive dependence with

$$\mathbf{M}_{t,s} = \begin{cases} 0, & s \leq t, \\ -\infty, & s > t, \end{cases} \Rightarrow \mathbf{A}_{t,s}^{(l,h)} = 0 \text{ for } s > t, \quad \sum_{s \leq t} \mathbf{A}_{t,s}^{(l,h)} = 1. \quad (3)$$

Thus, each attention map $\mathbf{A}^{(l,h)} \in \mathbb{R}^{T \times T}$ is lower-triangular and row-stochastic, providing head-specific weights over past positions that we analyze.

3.2 Reinforcement Learning with Verifiable Rewards

RL optimized the LLM policy to maximize the cumulative rewards r received from the verifier:

$$\max_{\theta} \mathcal{J}(\theta) := \mathbb{E}_{\mathbf{q} \sim Q, \mathbf{o} \sim \pi_{\theta}(\cdot|\mathbf{q})} [r(\mathbf{o})]. \quad (4)$$

Policy gradient methods (Williams, 1992) are a standard approach for solving this optimization problem, with Proximal Policy Optimization (PPO) (Schulman et al., 2017) as the de facto standard for stable, sample-efficient fine-tuning. PPO updates on data from a frozen old policy π_{old} , applies importance sampling to correct distribution shift, and optimizes a clipped surrogate objective to constrain divergence between the new and old policies:

$$\mathcal{J}_{PPO}(\theta) = \mathbb{E}_{\mathbf{q} \sim Q, \mathbf{o} \sim \pi_{\theta}(\cdot|\mathbf{q})} \frac{1}{|\mathbf{o}|} \sum_{t=1}^{|\mathbf{o}|} \min \left(\frac{\pi_{\theta}(o_t|\mathbf{q}, \mathbf{o}_{<t})}{\pi_{\theta_{old}}(o_t|\mathbf{q}, \mathbf{o}_{<t})} A_t, \text{clip} \left(\frac{\pi_{\theta}(o_t|\mathbf{q}, \mathbf{o}_{<t})}{\pi_{\theta_{old}}(o_t|\mathbf{q}, \mathbf{o}_{<t})}, 1-\epsilon, 1+\epsilon \right) A_t \right) \quad (5)$$

where A_t is the advantage at step t , typically estimated via Generalized Advantage Estimation (GAE) (Schulman et al., 2015), and ϵ is a clipping hyperparameter for stabilizing updates.

Group Relative Policy Optimization (GRPO) (Shao et al., 2024) eliminates the value function (critic) and instead estimates the advantage by normalizing rewards within a group of sampled responses for the same prompt. Specifically, for a prompt \mathbf{q} with G responses and associated rewards $\{r_i\}_{i=1}^G$, the group-normalized advantage is given by:

$$\hat{A}_{i,t} = \frac{r_i - \text{mean}(\{r_i\}_{i=1}^G)}{\text{std}(\{r_i\}_{i=1}^G)}. \quad (6)$$

By emphasizing the differences among candidate outputs for the same prompt, it effectively preserves the reliability of the gradient signal, even in sparse reward settings. In addition to this modified advantage estimation, GRPO adds a KL penalty term to the clipped objective in Eq. 5.

4 Dissecting Attention Dynamics to Expose the Reasoning Rhythm

This section dissects attention dynamics to uncover an intrinsic rhythm in model reasoning and grounds each claim with **inline empirical validations**. More experimental details can be found in Appendix A.1.

4.1 Head Grouping by Span and the Emergent Local/Global Patterns

To uncover characteristic reasoning patterns, we analyze attention maps from two complementary directions, i.e., forward (the reach of a token’s downstream influence into distant later steps) and backward (the extent to which a token’s generation is dominated by the immediately preceding context). Together, these perspectives correspond to local and global views of the reasoning structure.

We analyze attention dynamics using Qwen3-4B-Base (Yang et al., 2025a) on math prompts from the GSM8K dataset (Cobbe et al., 2021b) with temperature $T=0.7$. Using the non-SFT model avoids confounds from supervised instructions and provides a clean starting point for zero-RL training. For each prompt, we obtain attention maps via a single forward pass over the concatenated prompt-response sequence; unless otherwise noted, all token-level metrics are computed on rows corresponding to response tokens.

Let $\mathbf{A}^{(l,h)} \in \mathbb{R}^{N \times N}$ denote the causal attention map for layer l and head h over the full sequence of length N , with $\mathbf{A}_{t,s}^{(l,h)}$ the attention from position t to $s \leq t$. Since the attention is causal and row-stochastic ($\sum_{s=1}^t \mathbf{A}_{t,s}^{(l,h)} = 1$ for each t), we can interpret each row as a probability distribution over past positions. To characterize the effective receptive span of a head, we define its attention-weighted mean backward distance over the generated response positions \mathcal{R} as:

$$d^{(l,h)} = \frac{1}{|\mathcal{R}|} \sum_{t \in \mathcal{R}} \sum_{s=1}^t \mathbf{A}_{t,s}^{(l,h)} (t-s), \quad (7)$$

Since the inner sum is a convex combination of distances $(t-s)$, $d^{(l,h)}$ is precisely the average distance that head (l,h) looks back when generating tokens in the response. Consequently, heads with smaller $d^{(l,h)}$ indicate a strong focus toward recent context (i.e., attention concentrated near the diagonal), reflecting local focus, whereas large values signify frequent long-range dependencies (i.e., attention reaching far into the past), characteristic of global focus. We sort all heads by $d^{(l,h)}$ and designate the lowest and highest

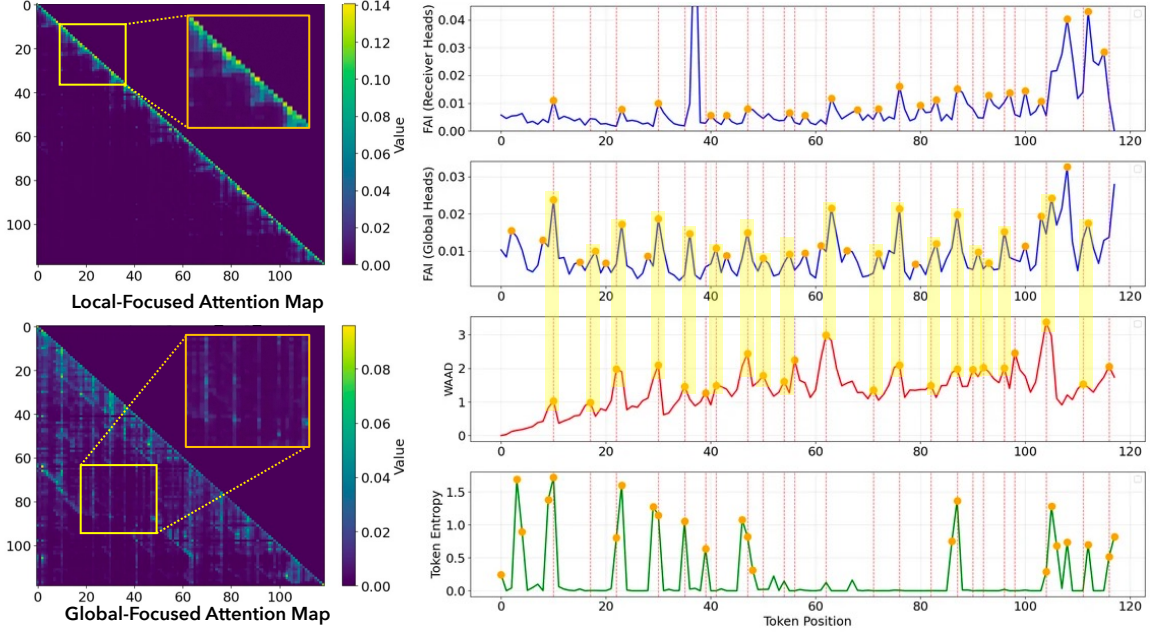


Figure 2: Visualization and quantification of local and global attention patterns on a math reasoning case. Left: a local-focused attention map highlights near-diagonal sawtooth patterns, and a global-focused map highlights vertical stripes indicative of broader attention. Right: the corresponding token-level metrics, including FAI (Def. 4.1) for receiver and global heads, WAAD (Def. 4.1), and token entropy, with key points correlating with each other.

quantiles (e.g., bottom/top 30%) as the local-focused set \mathcal{H}_{loc} and global-focused set $\mathcal{H}_{\text{glob}}$, respectively. We then aggregate attention within each group:

$$\bar{\mathbf{A}}^{\text{loc}} = \frac{1}{|\mathcal{H}_{\text{loc}}|} \sum_{(l,h) \in \mathcal{H}_{\text{loc}}} \mathbf{A}^{(l,h)}, \quad \bar{\mathbf{A}}^{\text{glob}} = \frac{1}{|\mathcal{H}_{\text{glob}}|} \sum_{(l,h) \in \mathcal{H}_{\text{glob}}} \mathbf{A}^{(l,h)}. \quad (8)$$

Fig. 2 visualizes $\bar{\mathbf{A}}^{\text{loc}}$ and $\bar{\mathbf{A}}^{\text{glob}}$, revealing two complementary patterns summarized below.

Local Attention Pattern: Near-Diagonal Sawtooth Indicating Local Phrasal Chunks. The local-focused aggregate map $\bar{\mathbf{A}}^{\text{loc}}$ exhibits a characteristic sawtooth along the diagonal that tracks phrasal or semantic chunks. Within a semantic or phrasal chunk (e.g., “by the way”), attention remains tightly local, while at the onset of a new chunk, attention abruptly reaches further back, followed by locally dominated tokens.

To operationalize this local structure, we introduce a windowed distance to measure how far a token looks back within a clipped window, emphasizing whether the model must reach beyond immediate neighbors to resolve ambiguity. We introduce a time window to downweight absolute positional artifacts since tokens of different positions handle different preceding attention ranges.

Definition 1: Windowed Average Attention Distance (WAAD)

For a response position $t \in \mathcal{R}$, with a small clipping window W ,

$$\text{WAAD}_t = \sum_{s=1}^t \bar{\mathbf{A}}_{t,s}^{\text{loc}} \min(t-s, W). \quad (9)$$

Low WAAD values indicate tight local continuation within a chunk (valleys), while spikes represent long-range consultation at chunk boundaries (peaks). The WAAD sequence in Fig. 2 reveals clear peak-valley alternation aligned with chunk boundaries: a chunk onset typically exhibits a peak (it must retrieve earlier context to form semantics), followed by a sharp drop as subsequent tokens rely on immediate neighbors. Mechanistically, local heads enact habit-driven micro-syntax, where once a chunk is initiated, subsequent tokens are locally licensed with low uncertainty, reflecting collocational continuations internalized during pretraining. Hesitation concentrates at chunk boundaries, where the model consults longer-range context.

Global Attention Pattern: Sparse Anchors with Broad Influence to Downstream Tokens. The global-

focused aggregate map \bar{A}^{glob} disproportionately highlights a sparse set of tokens that receive sustained attention from many future positions. These tokens function as semantic anchors that are repeatedly revisited and steer unfolding reasoning to a stable frame. We quantify a token’s downstream importance by averaging the attention it receives from future positions within a controlled horizon.

Definition 2: Future Attention Influence

For a token s , let H_{lo} and H_{hi} be lower/upper horizons for influence calculation. With the index set defined as $\mathcal{T}(s) = \{t \mid t \in \mathcal{R}, s+H_{\text{lo}} \leq t \leq \min(N, s+H_{\text{hi}})\}$,

$$\text{FAI}_s = \frac{1}{|\mathcal{T}(s)|} \sum_{t \in \mathcal{T}(s)} \bar{A}_{t,s}^{\text{glob}}. \tag{10}$$

High FAI surfaces tokens with broad downstream reach (anchor tokens). As shown in Fig. 2, visualizing FAI over a response reveals differences and fluctuations in token influence, where high-influence tokens essentially correspond to key logical waypoints (e.g., pivotal definitions, intermediate results, or decision points). We also observe a growing density of high-FAI tokens as the trajectory approaches the final answer region, consistent with the need to consolidate prior reasoning.

Do Perturbations at High-FAI Tokens More Effectively Alter Subsequent Reasoning? At a chosen position i^* , we take the predictive distribution $p_\theta(\cdot \mid \mathbf{o}_{<i^*})$, select the top- k candidates $\mathcal{V}_k(i^*)$ (i.e., highest-logit tokens), and for each $v \in \mathcal{V}_k(i^*)$ we force $o_{i^*} = v$ and roll out continuations under greedy decoding. We then compare each counterfactual trajectory $\tilde{\mathbf{o}}_{>i^*}^v$ with the original $\mathbf{o}_{>i^*}$ using Jaccard overlap over content words, with $\mathcal{S}(\cdot)$ denotes the content token set of a reasoning trajectory:

$$\text{Jaccard}(\mathbf{o}_{>i^*}, \tilde{\mathbf{o}}_{>i^*}^v) = \frac{|\mathcal{S}(\mathbf{o}_{>i^*}) \cap \mathcal{S}(\tilde{\mathbf{o}}_{>i^*}^v)|}{|\mathcal{S}(\mathbf{o}_{>i^*}) \cup \mathcal{S}(\tilde{\mathbf{o}}_{>i^*}^v)|}. \tag{11}$$

We conduct this analysis on 70 randomly sampled math problems. We conduct rollout simulations on high-FAI positions and low-FAI positions for comparison. As shown in Table 1, across problems and rollout horizons, perturbations at high-FAI positions yield substantially lower Jaccard similarity, with 87.14% of trials showing greater deviation than at low-FAI positions. This indicates that FAI-identified anchors causally organize downstream inference: changing them reshapes the global plan and cadence of reasoning, whereas interventions at locally dominated positions primarily affect surface form without redirecting the overall trajectory.

Table 1: Jaccard similarity of rollouts for top- and bottom- k ranked by FAI. $\text{Pr}(\text{Top} < \text{Bottom})$ denotes the percentage of trials where top- k similarity is lower.

	Top- k	Bottom- k
Mean Jaccard similarity	0.534	0.631
$\text{Pr}(\text{Top} < \text{Bottom})$	87.14%	

Fig. 3 and the corresponding results in Appendix B.1 show examples comparing the effects of perturbing high-FAI versus low-FAI positions. Replacing high-FAI tokens (even with semantically similar alternatives) frequently induces substantial shifts in the model’s downstream reasoning logic, such as altering the problem-solving strategy or even changing the overall correctness, as reflected by the low Jaccard similarity. In contrast, perturbations at low-FAI positions typically affect only local phrasing while preserving the global reasoning structure, even yielding near-identical continuations. The results show that FAI reflects a reasoning-anchoring capacity that causally governs the model’s planning and execution rhythm, rather than merely reflecting surface-level linguistic variation.

4.2 Joint Dynamics: A Recurring Preplan-and-Anchor Mechanism

Single-metric evaluations of reasoning often provide an incomplete picture. In practice, key internal signals are closely coupled. This section explores the joint dynamics of internal metrics while also connecting to readily observable indicators. A multidimensional analysis of these signals uncovers three robust empirical couplings, converging on a recurring preplan-and-anchor mechanism that underlies and organizes the model’s reasoning behavior.

Coupling Pattern 1: WAAD Peaks Maintain Higher Token Entropies. Token-level entropy $H_t = -\sum_v p_\theta(v \mid \mathbf{q}, \mathbf{o}_{<t}) \log p_\theta(v \mid \cdot)$ reflects predictive uncertainty and drives reasoning exploration (Wang et al., 2025b). As shown in Fig. 2, spikes in WAAD_t correspond to tokens with higher H_t . When immediate local cues dominate, next-token prediction is confident (low H_t) and attention remains near-diagonal (low WAAD_t), which is consistent with habit-driven micro-syntax learned in pretraining (e.g., after “by the”, “way” follows naturally). In contrast, at semantic junctures where the local context underdetermines

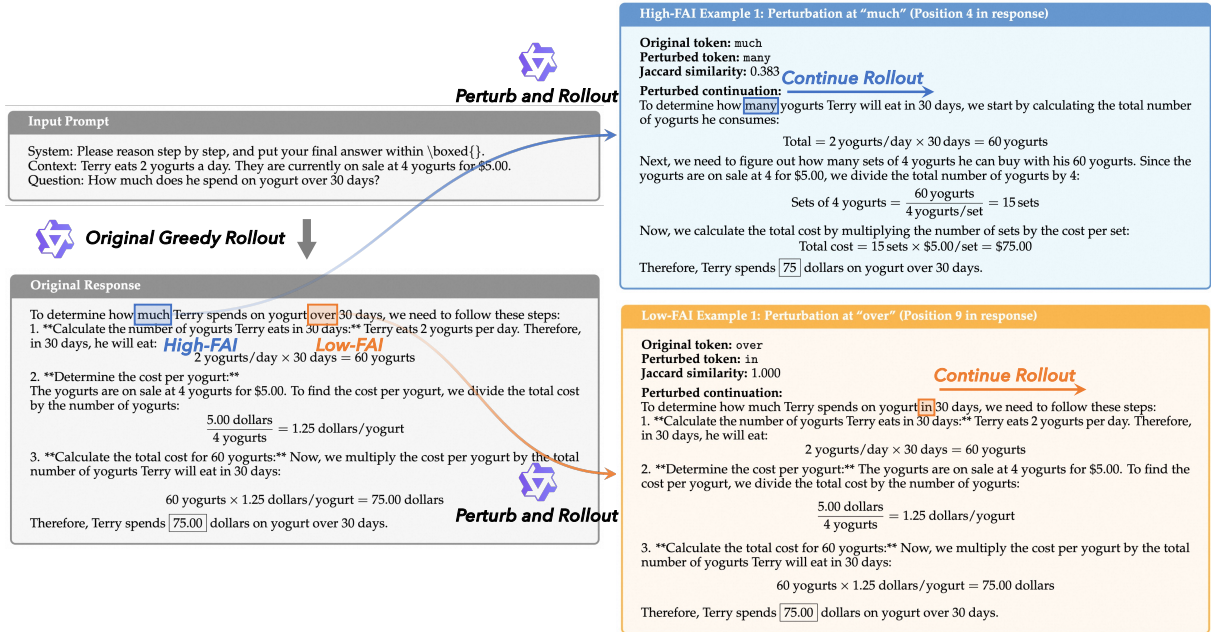


Figure 3: An example comparing the effects of perturbing high-FAI versus low-FAI positions and continuing the rollout of the subsequent reasoning trajectory. Perturbing a high-FAI position typically leads to a clear shift in the overall reasoning logic, whereas replacing a low-FAI token more frequently just alters local phrasing, leaving the downstream reasoning trajectory essentially unchanged.

the next step, the model exhibits higher uncertainty (high H_t) and reaches further back to retrieve disambiguating information (high $WAAD_t$). In this sense, high-entropy tokens and $WAAD$ peaks can be two sides of the same coin: local ambiguity triggers long-range consultation. Conversely, locally dominated tokens tend to have lower entropy, reflecting stereotyped continuations that can be decided from local context alone.

Coupling Pattern 2: Receiver Heads and Global-Focused Heads Surface Shared Anchors. Bogdan et al. (2025) has identified receiver heads, i.e., attention heads whose inbound attention distribution is highly selective and thus diagnostic of tokens that attract strong attention from future positions (e.g., via column-wise kurtosis). We compare those heads with our global-focused set $\mathcal{H}_{\text{glob}}$, and find that the token-level downstream influence computed from either set is highly concordant. Aggregating attention over receiver heads or over $\mathcal{H}_{\text{glob}}$ yields strongly correlated FAI profiles across tokens, as shown in Fig. 2, indicating that span-based and kurtosis-based filtering arrive at the same conclusions and mutually corroborate one another.

Coupling Pattern 3: FAI Peaks Follow or Coincide with $WAAD$ Peaks. As highlighted in Fig. 2, high-FAI tokens typically occur at or just after $WAAD$ peaks, reflecting a two-beat process: (i) *Preplan*: As the model approaches a semantic boundary, a $WAAD$ peak signals long-range context retrieval to generate an introductory token that prepares the forthcoming concept or step. (ii) *Anchor*: At the same position or immediately later, the model emits a token with high FAI, repeatedly attended by future positions to guide and stabilize subsequent reasoning. When the model delivers a key logical point, it may have already planned it in advance; however, to preserve fluency and conventional phrasing, it often first produces an introductory token to open the chunk and only then emits the key anchor token. From a local perspective, such anchor tokens can be dominated by immediately preceding tokens, leaving little room for exploration at the anchor position itself. This motivates joint consideration of both the anchor and its introductory token during optimization.

Quantitative Analysis. To quantify the significance of the three couplings, we randomly sample 70 questions and analyze linkages between metrics. For each coupling, we compute the observed statistic (e.g., average entropy at $WAAD$ peaks, co-occurrence rates of FAI and receiver-head peaks, alignment between $WAAD$ and FAI peaks) and compare it against the expectation under random situations in which the positions of the first metric’s peaks are shuffled. Table 2 shows that all couplings exhibit substantial lifts over random chance (ranging from +42.47% to +171.49%), validating these joint dynamics.

Table 2: Quantitative Analysis of Linkages Between Key Metrics. Random baselines are illustrative estimates based on the probability of this value occurring under completely random conditions. Lift quantifies the strength of the correlation beyond random chance, calculated by (Observed - Random)/Random.

	Metric Correlation	Random	Observed	Lift
	Average Entropy of the WAAD Peaks	0.2386	0.3608	+51.97%
	FAI Peak of Receiver & Global Heads Co-occurrence	22.41%	60.84%	+171.49%
	FAI Peak Follows/Coincides with WAAD Peak	36.87%	52.53%	+42.47%

5 Fine-Grained Policy Optimization Driven by Attention Signals

Conventional sequence-level RLVR distributes credit uniformly across tokens, overlooking the internal reasoning organization that indicates positions (preplans and anchors) are structurally decisive. We instead align token-level credit with the model’s intrinsic reasoning rhythm by rescaling the per-token advantage in on-policy RL using data-dependent weights derived from attention dynamics.

5.1 Attention Calculation in the RL Framework

The Vanilla RL Framework. In reinforcement learning (RL) for large language models (LLMs), the core objective is to optimize a policy that maximizes expected task-specific rewards, such as correctness in mathematical reasoning, while maintaining alignment with the original language distribution. Under PPO framework, which also generalizes to GRPO and similar on-policy methods, training proceeds through an iterative loop of inference, reward evaluation, and policy update. We implement our methods on top of the ROLL framework (Wang et al., 2025c).

In our setup, two reasoning model instances are maintained: (1) `actor_infer`: deployed with vLLM for high-throughput, low-latency inference; (2) `actor_train`: implemented in Megatron for efficient large-scale training with model parallelism. At each iteration, `actor_infer` (initialized from the latest `actor_train` weights) generates a batch of responses to input prompts. These responses are evaluated by a reward model or an execution-based verifier, producing scalar rewards per sequence. The prompt-response-reward tuples constitute the RL experience data. This data is then fed to `actor_train`, which computes policy gradients using the clipped objective to ensure stable updates. After each training update, the updated weights of `actor_train` are synchronized to `actor_infer`, closing the loop.

Implementation of Attention Mechanisms in RL. Modern distributed training frameworks and inference engines for LLM like vLLM and Megatron typically employ flash attention (Dao et al., 2022) for computational efficiency, which discards full attention matrices during execution to reduce memory overhead. Consequently, the complete attention maps are not available for analysis in either `actor_infer` or `actor_train`. To address this, we introduce a dedicated auxiliary model, `actor_attn`, implemented with a standard Transformer. This model retains full attention weights during the forward pass, enabling us to compute internal metrics based on attention dynamics.

Specifically, after `actor_infer` completes generation of a response (which involves hundreds to thousands of forward steps during autoregressive decoding), we concatenate the original prompt and the generated response into a single sequence and perform one additional forward pass through `actor_attn`. During this pass, we sample attention maps from five evenly spaced layers within the middle third of the network (i.e., from layers $\lfloor L/3 \rfloor$ to $\lfloor 2L/3 \rfloor$, where L is the total number of layers) to serve as representative snapshots of the model’s internal attention behavior. The model typically requires thousands of forward passes for token-by-token generation, whereas we obtain attention maps with just a single additional forward pass over the generated response (together with the prompt), introducing little additional latency with parallel computation. After each policy update of `actor_train`, its parameters are synchronized to both `actor_infer` and `actor_attn` to ensure consistency across inference, training, and attention analysis.

5.2 Targeted Credit Assignment to Critical Nodes in Reasoning

For the specific advantage scaling designs in RL, without loss of generality, we illustrate with the vanilla PPO objective and introduce a shaped advantage:

$$\mathcal{J}(\theta) = \mathbb{E}_{\mathbf{q} \sim Q, \mathbf{o} \sim \pi_{\theta}(\cdot|\mathbf{q})} \frac{1}{|\mathbf{o}|} \sum_{t=1}^{|\mathbf{o}|} \min \left(\frac{\pi_{\theta}(\mathbf{o}_t|\mathbf{q}, \mathbf{o}_{<t})}{\pi_{\theta_{\text{old}}}(\mathbf{o}_t|\mathbf{q}, \mathbf{o}_{<t})} A_t \gamma_t, \text{clip} \left(\frac{\pi_{\theta}(\mathbf{o}_t|\mathbf{q}, \mathbf{o}_{<t})}{\pi_{\theta_{\text{old}}}(\mathbf{o}_t|\mathbf{q}, \mathbf{o}_{<t})}, 1-\epsilon, 1+\epsilon \right) A_t \gamma_t \right) \quad (12)$$

where γ_t is the scaling coefficient. Our variants amplify the advantages of tokens identified by the model’s internal reasoning patterns, thereby improving the efficiency of RL. We instantiate γ_t with three

strategies that correspond to the local preplan signal, the global anchor signal, and their joint coupling.

(1) Local-chunk credit: select preplan tokens via distance drops, motivated by the local attention pattern (Sec. 4.1). For the tokens within each response, we detect preplan tokens by the WAAD variations between consecutive positions and then select the top q quantile tokens accordingly:

$$\Delta_t = |\text{WAAD}_t - \text{WAAD}_{t+1}| \quad \text{and} \quad \mathcal{T}_{\text{loc}} = \text{TopQ}(\Delta_t, q=0.4), \quad (13)$$

Here, large Δ_t identifies the boundary tokens at a peak-valley transition of phrasal chunks. Since these tokens initiate local scaffolds and guide subsequent reasoning, emphasizing these points strengthens the locus of planning and encourages the policy to resolve long-range dependencies before committing. We amplify advantages of tokens within \mathcal{T}_{loc} by configuring the scaling coefficient:

$$\gamma_t = 1 + (\gamma_{\text{amp}} - 1) \mathbf{1}\{t \in \mathcal{T}_{\text{loc}}\}, \quad (14)$$

where $\gamma_{\text{amp}} = 1.5$ denotes an amplification factor.

(2) Global-anchor credit: select tokens with high future influence, motivated by the global attention pattern (Sec. 4.1). We score tokens by FAI and then select the top q quantile tokens accordingly:

$$\mathcal{T}_{\text{glob}} = \text{TopQ}(\text{FAI}, q=0.4), \quad (15)$$

By amplifying anchors, it learns to articulate and preserve core semantic commitments that organize downstream inference. Because these tokens largely determine subsequent reasoning, prioritizing reinforcement (and, when applicable, penalties) at these positions propagates the verifiable signal to the key points more quickly, enabling more targeted optimization. Thus, We amplify advantages of tokens within $\mathcal{T}_{\text{glob}}$ by configuring the scaling coefficient:

$$\gamma_t = 1 + (\gamma_{\text{amp}} - 1) \mathbf{1}\{t \in \mathcal{T}_{\text{glob}}\}, \quad (16)$$

where $\gamma_{\text{amp}} = 1.5$ denotes an amplification factor.

(3) Coupled rhythm credit: combine preplans and anchors, and back-allocate credit from anchors to their local precursors, motivated by the joint dynamic of local/global patterns (Sec. 4.2). A locally dominated anchor has limited freedom to optimize, so we back-allocate credit of high-FAI tokens across the local semantic chunk, promoting coherent chunk-level scaffolding rather than overfitting to a single position. We couple WAAD with FAI signal to reflect the two-beat rhythm and to share credit between anchors and their preceding preplans. The key idea is: identify high-influence anchors, test whether they are locally dominated, and, if so, diffuse a fraction of their credit backward to the preplan token that prepares the anchor.

With the anchor candidate set $\mathcal{T}_{\text{glob}}$, the WAAD variations Δ_t , and given thresholds τ_{waad} and τ_{Δ} , we say an anchor t is locally dominated by its immediate past k tokens if

$$\text{WAAD}_t \leq \tau_{\text{waad}} \quad \text{and} \quad \max_{u \in \{t-k, \dots, t-1\}} \Delta_u \geq \tau_{\Delta}. \quad (17)$$

We denote $t \in \mathcal{D}$ when t is a high-influence token with low WAAD, locally licensed preceded by a recent WAAD peak. Then, we redistribute a fraction $\alpha \in [0, 1]$ of the amplification bonus $\gamma_{\text{amp}} - 1$ from each locally dominated anchor to its associated introductory token $\mathcal{I}(\mathcal{D}) = \{\text{intro}(s) : s \in \mathcal{D}\}$:

$$\gamma_t = 1 + (\gamma_{\text{amp}} - 1) \mathbf{1}\{t \in \mathcal{T}_{\text{glob}} \setminus \mathcal{D}\} + (1 - \alpha)(\gamma_{\text{amp}} - 1) \mathbf{1}\{t \in \mathcal{D}\} + \alpha(\gamma_{\text{amp}} - 1) \mathbf{1}\{t \in \mathcal{I}(\mathcal{D})\}, \quad (18)$$

where $\gamma_{\text{amp}} = 1.5$ denotes an amplification factor.

5.3 Experimental Evaluation

5.3.1 Experiment Settings

Benchmarks. We test on relatively simple puzzles and question-answering (QA) benchmarks and challenging mathematical reasoning datasets. (i) the *Countdown* puzzle (Pan et al., 2025), where the goal is to combine four given numbers using arithmetic operations to reach a target value; (ii) the *CrossThink-QA* dataset (Akter et al., 2025), which aggregates multi-domain QA pairs from heterogeneous sources; and (iii) five standard math reasoning benchmarks: AIME24, AIME25, AMC, MATH500 (Hendrycks et al., 2021), and OlympiadBench (He et al., 2024).

Baselines. Our approach introduces a novel modulation of token-level advantages for RL. To isolate the impact of this design, we implement our method on top of GRPO to directly assess the improvement. In addition, we consider alternative token-level advantage enhancement strategies for comparison: (1)

Table 3: Results on the Countdown and QA datasets. Bold denotes the best results per dataset.

Method	Countdown	CrossThinkQA
GRPO	52.6	48.0
+ random credit	55.0	47.8
+ high-entropy credit	57.7	48.0
+ local-chunk credit	59.9 +7.3	50.0 +2.0
+ global-anchor credit	60.4 +7.7	49.6 +1.6
+ coupled rhythm credit	63.1 +10.5	50.1 +2.1

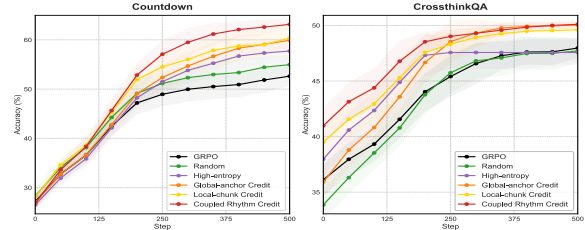


Figure 4: RL curves of Qwen3-4B-Base on Countdown and Qwen3-8B-Base on QA.

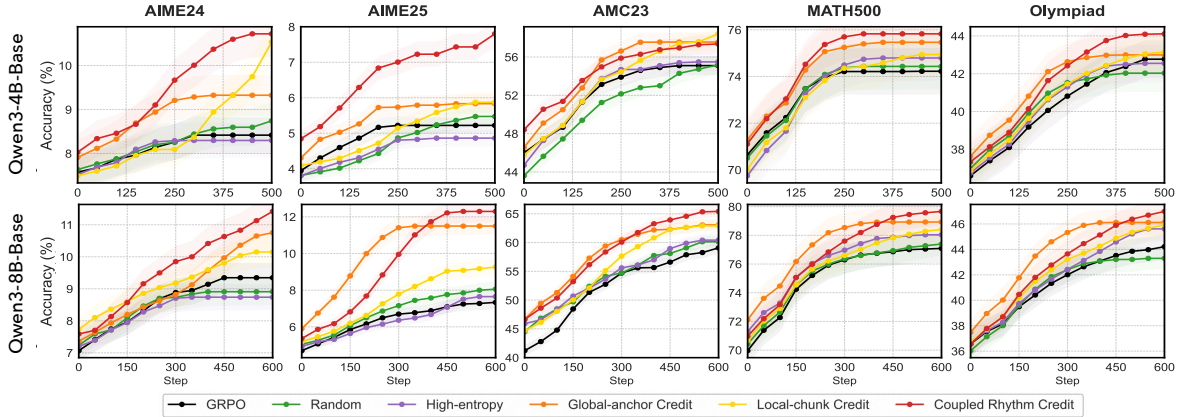


Figure 5: RL Performance curves of Qwen3-4B-Base and Qwen3-8B-Base models for math reasoning.

Random: randomly select tokens for advantage amplification; (2) *Entropy*: amplify advantages for tokens with high predictive entropy to encourage exploration.

Backbone Models and Implementation Details. Experiments are conducted using the Qwen3-4B-Base and Qwen3-8B-Base models. We use a maximum context length of 1024 for simple puzzles and QA, and 1024 or 8192 for math reasoning. The shorter context length is adopted as it yields a cleaner reasoning process that aligns more closely with the analytical environment and is less confounded by long-range dependencies that can dilute the effect of attention-based strategies. The curves are smoothed through the exponential moving averages of the peak performance, emphasizing sustained improvements.

Training details. We use a training batch size of 512 and micro-batch size of 32, yielding 16 gradient steps per batch, with learning rate 1×10^{-6} . The loss excludes both KL and entropy regularization. Decoding temperature during training is $T=1.0$. Our rhythm-aligned variants replace the per-token advantage A_t by $\tilde{A}_t = \gamma_t A_t$, where γ_t is computed from attention maps captured in a single forward pass. Unless noted, we set the WAAD window $W = 10$, the FAI horizon $H \in [10, 50]$, anchor selection by top-quantile ($q=40\%$), neighborhood size $k \in \{1, 2, 3\}$ for back-allocation. All shaping signals are detached from gradients and applied only to nonnegative advantages. The 4B models are trained on 8 GPUs, and the 8B models are trained on 16 GPUs, running for 500 and 600 steps, respectively. More experimental details for RL experiments can be found in Appendix A.2.

5.3.2 Results and Analyses

Results on Simple Logical Puzzles and QA. Table 3 reports the final accuracy on the Countdown and CrossThink-QA benchmarks. On Countdown, our *coupled rhythm credit* strategy achieves 63.1%, substantially outperforming GRPO (52.6%). Notably, both *local-chunk* and *global-anchor* credit schemes also yield consistent gains, suggesting that structured credit propagation effectively guides policy learning. In contrast, random or entropy-based token selection provides marginal or no improvement. On CrossThink-QA, where reasoning is more open-ended and less constrained by formal rules, all credit-aware variants show consistent improvements over GRPO (48.0%). The best-performing variant, *coupled rhythm credit*, reaches 50.1%, indicating that attention-based credit assignment can aid generalization in heterogeneous QA. Fig. 4 shows the training curves on Countdown and QA tasks. Our variants converge faster and reach higher plateaus than GRPO, with *coupled credit* exhibiting the earliest improvement and highest scores.

Results on Mathematical Reasoning. Table 4 evaluates credit assignment strategies across mathematical reasoning benchmarks and model scales. Our methods consistently outperform both the GRPO baseline and naive alternatives (e.g., random or high-entropy credit). Notably, *coupled rhythm credit* achieves the

Table 4: Results of math reasoning. AIME 24&25: avg@16; others: pass@1. Bold denotes the best results.

Method	AIME24	AIME25	AMC23	MATH	Olympiad	Avg.
<i>Qwen3-4B-Base with 1K Length</i>						
GRPO	8.4	5.2	55.1	74.2	42.8	37.1
+ random credit	8.7	5.5	55.2	74.4	42.0	37.1
+ high-entropy credit	8.3	4.9	55.5	74.8	42.5	37.2
+ global-anchor credit	9.3 +0.9	5.8 +0.6	57.6 +2.5	75.5 +1.2	43.0 +0.2	38.2 +1.1
+ local-chunk credit	10.5 +2.1	5.9 +0.7	58.4 +3.3	74.9 +0.7	43.1 +0.4	38.6 +1.5
+ coupled rhythm credit	10.7 +2.3	7.8 +2.6	57.4 +2.3	75.8 +1.6	44.1 +1.3	39.2 +2.1
<i>Qwen3-8B-Base with 1K Length</i>						
GRPO	9.3	7.3	59.1	77.1	44.2	39.4
+ random credit	8.9	8.1	60.1	77.4	43.3	39.6
+ high-entropy credit	8.7	7.7	60.4	78.0	45.6	40.1
+ global-anchor credit	10.8 +1.4	11.5 +4.2	63.1 +4.0	78.9 +1.8	46.1 +1.9	42.1 +2.7
+ local-chunk credit	10.1 +0.8	9.3 +1.9	62.9 +3.8	78.4 +1.3	45.9 +1.7	41.3 +1.9
+ coupled rhythm credit	11.4 +2.1	12.3 +5.0	65.4 +6.3	79.7 +2.6	47.0 +2.8	43.2 +3.8
<i>Qwen3-4B-Base with 8K Length</i>						
GRPO	19.5	16.1	57.6	81.0	49.9	44.8
+ random credit	18.0	16.6	57.1	82.0	50.0	44.7
+ high-entropy credit	19.3	15.4	57.8	81.2	48.6	44.5
+ global-anchor credit	21.7 +2.3	19.5 +3.4	61.1 +3.5	82.1 +1.2	51.2 +1.3	47.1 +2.3
+ local-chunk credit	22.4 +2.9	20.4 +4.3	59.2 +1.6	82.5 +1.5	51.5 +1.6	47.2 +2.4
+ coupled rhythm credit	22.0 +2.5	19.9 +3.8	59.3 +1.7	82.9 +1.9	52.2 +2.3	47.3 +2.5

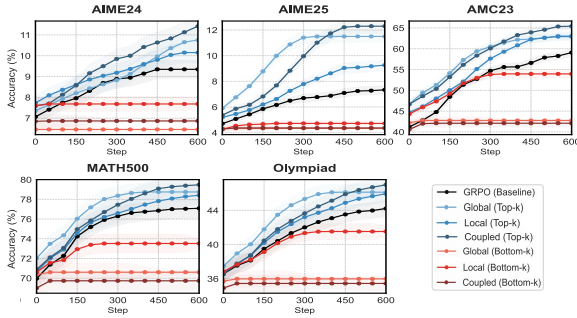


Figure 6: Peak performance moving averages of Top- k versus Bottom- k credit assignment.

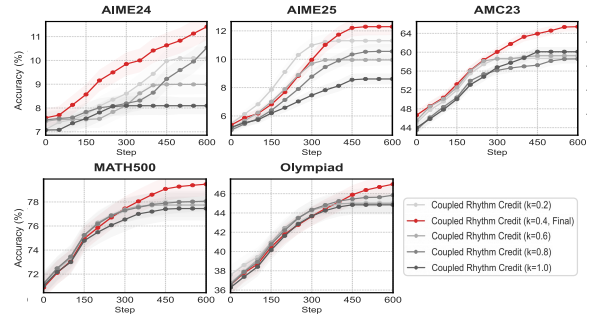


Figure 7: Performance curves of coupled rhythm credit by different Top- k ratios.

strongest gains across all settings, with the most pronounced improvements on challenging tasks for Qwen3-8B (e.g., +5.0pt on AIME25, +6.3pt on AMC23). These gains are robust across sequence lengths: with an extended 8K context, where base GRPO already benefits from longer reasoning traces, it still delivers consistent improvements (e.g., +4.3pt on AIME25). The curves in Fig. 5 further corroborate these findings, showing faster convergence and higher final performance for rhythm-aware credit strategies.

Ablation: Top- k versus Bottom- k . For proposed metrics, we experiment with reallocating additional credit to tokens ranked in the bottom 40% according to these metrics. Fig. 6 and Table 5 show that reinforcing credit on such low-scoring tokens (i.e., those locally dominated or exhibiting minimal global influence) leads to degraded performance. RL training becomes ineffective, and the peak evaluation metrics show no improvement on mathematical reasoning. In contrast, preferentially assigning credit to top- k tokens yields clear improvements. This contrast underscores the validity of our metric in identifying decisive positions.

Ablation: Top- k ratios. Fig. 7 shows the performance curves of our *coupled rhythm credit* with different top- k ratios, evaluated on multiple mathematical benchmarks using Qwen3-8B-Base. Table 5 shows the quantitative results. The results confirm that allocating credit exclusively to the top 40% of tokens (i.e., $k = 0.4$) yields the strongest overall performance, achieving the highest scores across all datasets and a peak average of 43.2. Both smaller ($k = 0.2$) and larger ($k \geq 0.6$) ratios lead to performance drops, indicating that reinforcing too few or too many tokens dilutes the signal for critical reasoning positions.

Table 5: Quantitative ablation results for Top-k vs. Bottom-k credit reallocation and different top-k ratios.

Method	AIME24	AIME25	AMC23	MATH500	Olympiad	Avg
GRPO (Baseline)	9.3	7.3	59.1	77.1	44.2	39.4
Global (Bottom-40%)	7.0 -2.3	4.8 -2.5	46.0 -13.1	71.2 -5.9	36.4 -7.8	33.1 -6.3
Local (Bottom-40%)	8.0 -1.3	5.1 -2.2	57.9 -1.2	74.8 -2.3	42.1 -2.1	37.6 -1.8
Coupled (Bottom-40%)	7.2 -2.1	4.7 -2.6	44.4 -14.7	70.3 -6.8	36.0 -8.2	32.5 -6.9
Global (Top-40%)	10.8 +1.4	11.5 +4.2	63.1 +4.0	78.9 +1.8	46.1 +1.9	42.1 +2.7
Local (Top-40%)	10.1 +0.8	9.3 +1.9	62.9 +3.8	78.4 +1.3	45.9 +1.7	41.3 +1.9
Coupled (Top-40%)	11.4 +2.1	12.3 +5.0	65.4 +6.3	79.7 +2.6	47.0 +2.8	43.2 +3.7
Coupled (Top-20%)	10.1	11.3	58.7	78.0	45.1	40.6
Coupled (Top-60%)	9.0	9.9	59.2	77.7	45.0	40.2
Coupled (Top-80%)	10.5	10.6	58.6	78.1	45.8	40.7
Coupled (Top-100%)	8.1	8.6	60.1	77.5	44.8	39.8

6 Conclusion

We show that analyzing attention dynamics provides a powerful new lens for understanding and directing LLM reasoning and post-training designs. By analyzing local and global attention, we uncover a recurring preplan-and-anchor rhythm in LLM reasoning: long-range consultation precedes anchor tokens that organize downstream inference. We formalize this with two metrics, WAAD and FAI, that identify preplan and anchor tokens. Using these signals, we design a targeted RL credit assignment that amplifies rewards on critical nodes: it emphasizes preplan tokens at chunk onsets, amplifies anchor tokens, and reallocates credit from locally dominant anchors to their corresponding preplan tokens. The method is plug-and-play with standard RLVR, and yields consistent empirical gains across reasoning benchmarks compared with uniform credit assignment. More broadly, attention both explains intrinsic model behaviors and prescribes targeted interventions, opening a path to more transparent, interpretable, and effective policy optimization of reasoning models.

Acknowledgment

This work was in part supported by NSFC 92370201 and Alibaba Group.

References

- Syeda Nahida Akter, Shrimai Prabhunoye, Matvei Novikov, Seungju Han, Ying Lin, Evelina Bakhturina, Eric Nyberg, Yejin Choi, Mostofa Patwary, Mohammad Shoeybi, et al. Nemotron-crossthink: Scaling self-learning beyond math reasoning. *arXiv preprint arXiv:2504.13941*, 2025.
- Emmanuel Ameisen, Jack Lindsey, Adam Pearce, Wes Gurnee, Nicholas L. Turner, Brian Chen, Craig Citro, David Abrahams, Shan Carter, Basil Hosmer, Jonathan Marcus, Michael Sklar, Adly Templeton, Trenton Bricken, Callum McDougall, Hoagy Cunningham, Thomas Henighan, Adam Jermy, Andy Jones, Andrew Persic, Zhenyi Qi, T. Ben Thompson, Sam Zimmerman, Kelley Rivoire, Thomas Conerly, Chris Olah, and Joshua Batson. Circuit tracing: Revealing computational graphs in language models. *Transformer Circuits Thread*, 2025. URL <https://transformer-circuits.pub/2025/attribution-graphs/methods.html>.
- Yuntao Bai, Andy Jones, Kamal Ndousse, Amanda Askell, Anna Chen, Nova DasSarma, Dawn Drain, Stanislav Fort, Deep Ganguli, Tom Henighan, et al. Training a helpful and harmless assistant with reinforcement learning from human feedback. *arXiv preprint arXiv:2204.05862*, 2022a.
- Yuntao Bai, Saurav Kadavath, Sandipan Kundu, Amanda Askell, Jackson Kernion, Andy Jones, Anna Chen, Anna Goldie, Azalia Mirhoseini, Cameron McKinnon, Carol Chen, Catherine Olsson, Christopher Olah, Danny Hernandez, Dawn Drain, Deep Ganguli, Dustin Li, Eli Tran-Johnson, Ethan Perez, Jamie Kerr, Jared Mueller, Jeffrey Ladish, Joshua Landau, Kamal Ndousse, Kamile Lukosuite, Liane Lovitt, Michael Sellitto, Nelson Elhage, Nicholas Schiefer, Noemi Mercado, Nova DasSarma, Robert Lasenby, Robin Larson, Sam Ringer, Scott Johnston, Shauna Kravec, Sheer El Showk, Stanislav Fort, Tamera Lanham, Timothy Telleen-Lawton, Tom Conerly, Tom Henighan, Tristan Hume, Samuel R. Bowman, Zac Hatfield-Dodds, Ben Mann, Dario Amodei, Nicholas Joseph, Sam McCandlish, Tom Brown, and Jared Kaplan. Constitutional ai: Harmlessness from ai feedback, 2022b. URL <https://arxiv.org/abs/2212.08073>.
- Federico Barbero, Ivaro Arroyo, Xiangming Gu, Christos Perivolaropoulos, Michael Bronstein, Petar Velickovi, and Razvan Pascanu. Why do llms attend to the first token?, 2025. URL <https://arxiv.org/abs/2504.02732>.
- Leonardo Bertolazzi, Philipp Mondorf, Barbara Plank, and Raffaella Bernardi. The validation gap: A mechanistic analysis of how language models compute arithmetic but fail to validate it, 2025. URL <https://arxiv.org/abs/2502.11771>.
- Paul C Bogdan, Uzay Macar, Neel Nanda, and Arthur Conmy. Thought anchors: Which llm reasoning steps matter? *arXiv preprint arXiv:2506.19143*, 2025.
- Vivien Cabannes, Charles Arnal, Wassim Bouaziz, Xingyu Yang, Francois Charton, and Julia Kempe. Iteration head: A mechanistic study of chain-of-thought. *Advances in Neural Information Processing Systems*, 37:109101–109122, 2024.
- Mark Chen, Jerry Tworek, Heewoo Jun, Qiming Yuan, Henrique Ponde De Oliveira Pinto, Jared Kaplan, Harri Edwards, Yuri Burda, Nicholas Joseph, Greg Brockman, et al. Evaluating large language models trained on code. *arXiv preprint arXiv:2107.03374*, 2021.
- Qiguang Chen, Libo Qin, Jiaqi Wang, Jinxuan Zhou, and Wanxiang Che. Unlocking the capabilities of thought: A reasoning boundary framework to quantify and optimize chain-of-thought, 2024. URL <https://arxiv.org/abs/2410.05695>.
- Daixuan Cheng, Shaohan Huang, Xuekai Zhu, Bo Dai, Wayne Xin Zhao, Zhenliang Zhang, and Furu Wei. Reasoning with exploration: An entropy perspective. *arXiv preprint arXiv:2506.14758*, 2025.
- Paul F Christiano, Jan Leike, Tom Brown, Miljan Martic, Shane Legg, and Dario Amodei. Deep reinforcement learning from human preferences. *Advances in neural information processing systems*, 30, 2017.
- Karl Cobbe, Vineet Kosaraju, Mohammad Bavarian, Mark Chen, Heewoo Jun, Lukasz Kaiser, Matthias Plappert, Jerry Tworek, Jacob Hilton, Reiichiro Nakano, Christopher Hesse, and John Schulman. Training verifiers to solve math word problems. *arXiv preprint arXiv:2110.14168*, 2021a.
- Karl Cobbe, Vineet Kosaraju, Mohammad Bavarian, Mark Chen, Heewoo Jun, Lukasz Kaiser, Matthias Plappert, Jerry Tworek, Jacob Hilton, Reiichiro Nakano, et al. Training verifiers to solve math word problems. *arXiv preprint arXiv:2110.14168*, 2021b.

-
- Ganqu Cui, Yuchen Zhang, Jiacheng Chen, Lifan Yuan, Zhi Wang, Yuxin Zuo, Haozhan Li, Yuchen Fan, Huayu Chen, Weize Chen, Zhiyuan Liu, Hao Peng, Lei Bai, Wanli Ouyang, Yu Cheng, Bowen Zhou, and Ning Ding. The entropy mechanism of reinforcement learning for reasoning language models, 2025. URL <https://arxiv.org/abs/2505.22617>.
- Tri Dao, Dan Fu, Stefano Ermon, Atri Rudra, and Christopher Ré. Flashattention: Fast and memory-efficient exact attention with io-awareness. *Advances in neural information processing systems*, 35:16344–16359, 2022.
- Zhichen Dong, Zhanhui Zhou, Zhixuan Liu, Chao Yang, and Chaochao Lu. Emergent response planning in llms, 2025. URL <https://arxiv.org/abs/2502.06258>.
- Subhabrata Dutta, Joykirat Singh, Soumen Chakrabarti, and Tanmoy Chakraborty. How to think step-by-step: A mechanistic understanding of chain-of-thought reasoning. *arXiv preprint arXiv:2402.18312*, 2024.
- Kawin Ethayarajh, Winnie Xu, Niklas Muennighoff, Dan Jurafsky, and Douwe Kiela. Kto: Model alignment as prospect theoretic optimization. *arXiv preprint arXiv:2402.01306*, 2024.
- Kanishk Gandhi, Ayush Chakravarthy, Anikait Singh, Nathan Lile, and Noah D Goodman. Cognitive behaviors that enable self-improving reasoners, or, four habits of highly effective stars. *arXiv preprint arXiv:2503.01307*, 2025.
- Mor Geva, Jasmijn Bastings, Katja Filippova, and Amir Globerson. Dissecting recall of factual associations in auto-regressive language models, 2023. URL <https://arxiv.org/abs/2304.14767>.
- Xiangming Gu, Tianyu Pang, Chao Du, Qian Liu, Fengzhuo Zhang, Cunxiao Du, Ye Wang, and Min Lin. When attention sink emerges in language models: An empirical view, 2025. URL <https://arxiv.org/abs/2410.10781>.
- Daya Guo, Dejian Yang, Haowei Zhang, Junxiao Song, Ruoyu Zhang, Runxin Xu, Qihao Zhu, Shirong Ma, Peiyi Wang, Xiao Bi, et al. Deepseek-r1: Incentivizing reasoning capability in llms via reinforcement learning. *arXiv preprint arXiv:2501.12948*, 2025.
- Shangmin Guo, Biao Zhang, Tianlin Liu, Tianqi Liu, Misha Khalman, Felipe Llinares, Alexandre Rame, Thomas Mesnard, Yao Zhao, Bilal Piot, Johan Ferret, and Mathieu Blondel. Direct language model alignment from online ai feedback, 2024. URL <https://arxiv.org/abs/2402.04792>.
- Tingxu Han, Zhenting Wang, Chunrong Fang, Shiyu Zhao, Shiqing Ma, and Zhenyu Chen. Token-budget-aware llm reasoning, 2025. URL <https://arxiv.org/abs/2412.18547>.
- Chaoqun He, Renjie Luo, Yuzhuo Bai, Shengding Hu, Zhen Leng Thai, Junhao Shen, Jinyi Hu, Xu Han, Yujie Huang, Yuxiang Zhang, et al. Olympiadbench: A challenging benchmark for promoting agi with olympiad-level bilingual multimodal scientific problems. *arXiv preprint arXiv:2402.14008*, 2024.
- Dan Hendrycks, Collin Burns, Saurav Kadavath, Akul Arora, Steven Basart, Eric Tang, Dawn Song, and Jacob Steinhardt. Measuring mathematical problem solving with the math dataset. *arXiv preprint arXiv:2103.03874*, 2021.
- Binyuan Hui, Jian Yang, Zeyu Cui, Jiayi Yang, Dayiheng Liu, Lei Zhang, Tianyu Liu, Jiajun Zhang, Bowen Yu, Keming Lu, et al. Qwen2. 5-coder technical report. *arXiv preprint arXiv:2409.12186*, 2024.
- Carlos E Jimenez, John Yang, Alexander Wettig, Shunyu Yao, Kexin Pei, Ofir Press, and Karthik Narasimhan. Swe-bench: Can language models resolve real-world github issues? *arXiv preprint arXiv:2310.06770*, 2023.
- Nathan Lambert, Jacob Morrison, Valentina Pyatkin, Shengyi Huang, Hamish Ivison, Faeze Brahman, Lester James V Miranda, Alisa Liu, Nouha Dziri, Shane Lyu, et al. Tulu 3: Pushing frontiers in open language model post-training. *arXiv preprint arXiv:2411.15124*, 2024.
- Nathan Lambert, Jacob Morrison, Valentina Pyatkin, Shengyi Huang, Hamish Ivison, Faeze Brahman, Lester James V. Miranda, Alisa Liu, Nouha Dziri, Shane Lyu, Yuling Gu, Saumya Malik, Victoria Graf, Jena D. Hwang, Jiangjiang Yang, Ronan Le Bras, Oyvind Tafjord, Chris Wilhelm, Luca Soldaini, Noah A. Smith, Yizhong Wang, Pradeep Dasigi, and Hannaneh Hajishirzi. Tulu 3: Pushing frontiers in open language model post-training, 2025. URL <https://arxiv.org/abs/2411.15124>.
- Harrison Lee, Samrat Phatale, Hassan Mansoor, Thomas Mesnard, Johan Ferret, Kellie Lu, Colton Bishop, Ethan Hall, Victor Carbune, Abhinav Rastogi, et al. Rlaif vs. rlhf: Scaling reinforcement learning from human feedback with ai feedback. *arXiv preprint arXiv:2309.00267*, 2023.

-
- Dacheng Li, Shiyi Cao, Tyler Griggs, Shu Liu, Xiangxi Mo, Eric Tang, Sumanth Hegde, Kourosh Hakhamaneshi, Shishir G Patil, Matei Zaharia, et al. Llms can easily learn to reason from demonstrations structure, not content, is what matters! *arXiv preprint arXiv:2502.07374*, 2025.
- Jia Li, Edward Beeching, Lewis Tunstall, Ben Lipkin, Roman Soletskyi, Shengyi Huang, Kashif Rasul, Longhui Yu, Albert Q Jiang, Ziju Shen, et al. Numinamath: The largest public dataset in ai4maths with 860k pairs of competition math problems and solutions. *Hugging Face repository*, 13(9):9, 2024.
- Zicheng Lin, Tian Liang, Jiahao Xu, Qiuzhi Lin, Xing Wang, Ruilin Luo, Chufan Shi, Siheng Li, Yujiu Yang, and Zhaopeng Tu. Critical tokens matter: Token-level contrastive estimation enhances llm’s reasoning capability. *arXiv preprint arXiv:2411.19943*, 2024.
- Jack Lindsey, Wes Gurnee, Emmanuel Ameisen, Brian Chen, Adam Pearce, Nicholas L. Turner, Craig Citro, David Abrahams, Shan Carter, Basil Hosmer, Jonathan Marcus, Michael Sklar, Adly Templeton, Trenton Bricken, Callum McDougall, Hoagy Cunningham, Thomas Henighan, Adam Jermy, Andy Jones, Andrew Persic, Zhenyi Qi, T. Ben Thompson, Sam Zimmerman, Kelley Rivoire, Thomas Conerly, Chris Olah, and Joshua Batson. On the biology of a large language model. *Transformer Circuits Thread*, 2025. URL <https://transformer-circuits.pub/2025/attribution-graphs/biology.html>.
- Xiao Liu, Hao Yu, Hanchen Zhang, Yifan Xu, Xuanyu Lei, Hanyu Lai, Yu Gu, Hangliang Ding, Kaiwen Men, Kejuan Yang, et al. Agentbench: Evaluating llms as agents. *arXiv preprint arXiv:2308.03688*, 2023.
- Zihe Liu, Jiashun Liu, Yancheng He, Weixun Wang, Jiaheng Liu, Ling Pan, Xinyu Hu, Shaopan Xiong, Ju Huang, Jian Hu, et al. Part i: Tricks or traps? a deep dive into rl for llm reasoning. *arXiv preprint arXiv:2508.08221*, 2025.
- Yingwei Ma, Yue Liu, Yue Yu, Yuanliang Zhang, Yu Jiang, Changjian Wang, and Shanshan Li. At which training stage does code data help llms reasoning?, 2023. URL <https://arxiv.org/abs/2309.16298>.
- Aman Madaan and Amir Yazdanbakhsh. Text and patterns: For effective chain of thought, it takes two to tango. *arXiv preprint arXiv:2209.07686*, 2022.
- Tianyi Men, Pengfei Cao, Zhuoran Jin, Yubo Chen, Kang Liu, and Jun Zhao. Unlocking the future: Exploring look-ahead planning mechanistic interpretability in large language models, 2024. URL <https://arxiv.org/abs/2406.16033>.
- Yu Meng, Mengzhou Xia, and Danqi Chen. Simpo: Simple preference optimization with a reference-free reward. *Advances in Neural Information Processing Systems*, 37:124198–124235, 2024.
- Hosein Mohebbi, Willem Zuidema, Grzegorz Chrupaa, and Afra Alishahi. Quantifying context mixing in transformers, 2023. URL <https://arxiv.org/abs/2301.12971>.
- OpenAI. Learning to reason with llms, 2024. URL <https://openai.com/index/learning-to-reason-with-llms/>.
- OpenAI, :, Sandhini Agarwal, Lama Ahmad, Jason Ai, Sam Altman, Andy Applebaum, Edwin Arbus, Rahul K. Arora, Yu Bai, Bowen Baker, Haiming Bao, Boaz Barak, Ally Bennett, Tyler Bertao, Nivedita Brett, Eugene Brevdo, Greg Brockman, Sebastien Bubeck, Che Chang, Kai Chen, Mark Chen, Enoch Cheung, Aidan Clark, Dan Cook, Marat Dukhan, Casey Dvorak, Kevin Fives, Vlad Fomenko, Timur Garipov, Kristian Georgiev, Mia Glaese, Tarun Gogineni, Adam Goucher, Lukas Gross, Katia Gil Guzman, John Hallman, Jackie Hehir, Johannes Heidecke, Alec Helyar, Haitang Hu, Romain Huet, Jacob Huh, Saachi Jain, Zach Johnson, Chris Koch, Irina Kofman, Dominik Kundel, Jason Kwon, Volodymyr Kyrylov, Elaine Ya Le, Guillaume Leclerc, James Park Lennon, Scott Lessans, Mario Lezcano-Casado, Yuanzhi Li, Zhuohan Li, Ji Lin, Jordan Liss, Lily Liu, Jiancheng Liu, Kevin Lu, Chris Lu, Zoran Martinovic, Lindsay McCallum, Josh McGrath, Scott McKinney, Aidan McLaughlin, Song Mei, Steve Mostovoy, Tong Mu, Gideon Myles, Alexander Neitz, Alex Nichol, Jakub Pachocki, Alex Paino, Dana Palmie, Ashley Pantuliano, Giambattista Parascandolo, Jongsoo Park, Leher Pathak, Carolina Paz, Ludovic Peran, Dmitry Pimenov, Michelle Pokrass, Elizabeth Proehl, Huida Qiu, Gaby Raila, Filippo Raso, Hongyu Ren, Kimmy Richardson, David Robinson, Bob Rotsted, Hadi Salman, Suvansh Sanjeev, Max Schwarzer, D. Sculley, Harshit Sikchi, Kendal Simon, Karan Singhal, Yang Song, Dane Stuckey, Zhiqing Sun, Philippe Tillet, Sam Toizer, Foivos Tsimpourlas, Nikhil Vyas, Eric Wallace, Xin Wang, Miles Wang, Olivia Watkins, Kevin Weil, Amy Wendling, Kevin Whinnery, Cedric Whitney, Hannah Wong, Lin Yang, Yu Yang, Michihiro Yasunaga, Kristen Ying, Wojciech Zaremba, Wenting Zhan, Cyril Zhang, Brian Zhang, Eddie Zhang, and Shengjia Zhao. gpt-oss-120b & gpt-oss-20b model card, 2025. URL <https://arxiv.org/abs/2508.10925>.

-
- Long Ouyang, Jeffrey Wu, Xu Jiang, Diogo Almeida, Carroll Wainwright, Pamela Mishkin, Chong Zhang, Sandhini Agarwal, Katarina Slama, Alex Ray, et al. Training language models to follow instructions with human feedback. *Advances in neural information processing systems*, 35:27730–27744, 2022.
- Jiayi Pan, Junjie Zhang, Xingyao Wang, Lifan Yuan, Hao Peng, and Alane Suhr. Tinyzero. <https://github.com/Jiayi-Pan/TinyZero>, 2025. Accessed: 2025-01-24.
- Rafael Rafailov, Archit Sharma, Eric Mitchell, Christopher D Manning, Stefano Ermon, and Chelsea Finn. Direct preference optimization: Your language model is secretly a reward model. *Advances in neural information processing systems*, 36:53728–53741, 2023.
- Jie Ren, Qipeng Guo, Hang Yan, Dongrui Liu, Quanshi Zhang, Xipeng Qiu, and Dahua Lin. Identifying semantic induction heads to understand in-context learning, 2024. URL <https://arxiv.org/abs/2402.13055>.
- John Schulman, Philipp Moritz, Sergey Levine, Michael Jordan, and Pieter Abbeel. High-dimensional continuous control using generalized advantage estimation. *arXiv preprint arXiv:1506.02438*, 2015.
- John Schulman, Filip Wolski, Prafulla Dhariwal, Alec Radford, and Oleg Klimov. Proximal policy optimization algorithms. *arXiv preprint arXiv:1707.06347*, 2017.
- John Schulman, Barret Zoph, Christina Kim, Jacob Hilton, Jacob Menick, Jiayi Weng, Juan Felipe Ceron Uribe, Liam Fedus, Luke Metz, Michael Pokorny, et al. Chatgpt: Optimizing language models for dialogue. *OpenAI blog*, 2(4), 2022.
- Zhihong Shao, Peiyi Wang, Qihao Zhu, Runxin Xu, Junxiao Song, Xiao Bi, Haowei Zhang, Mingchuan Zhang, YK Li, Yang Wu, et al. Deepseekmath: Pushing the limits of mathematical reasoning in open language models. *arXiv preprint arXiv:2402.03300*, 2024.
- Zhiqing Sun, Yikang Shen, Qinhong Zhou, Hongxin Zhang, Zhenfang Chen, David Cox, Yiming Yang, and Chuang Gan. Principle-driven self-alignment of language models from scratch with minimal human supervision. *Advances in Neural Information Processing Systems*, 36:2511–2565, 2023.
- Kimi Team, Angang Du, Bofei Gao, Bowei Xing, Changjiu Jiang, Cheng Chen, Cheng Li, Chenjun Xiao, Chenzhuang Du, Chonghua Liao, et al. Kimi k1. 5: Scaling reinforcement learning with llms. *arXiv preprint arXiv:2501.12599*, 2025.
- Alexander Matt Turner, Lisa Thiergart, Gavin Leech, David Udell, Juan J. Vazquez, Ulisse Mini, and Monte MacDiarmid. Steering language models with activation engineering, 2024. URL <https://arxiv.org/abs/2308.10248>.
- Jean Vassoyan, Nathanaël Beau, and Roman Plaud. Ignore the kl penalty! boosting exploration on critical tokens to enhance rl fine-tuning. *arXiv preprint arXiv:2502.06533*, 2025.
- Constantin Venhoff, Iván Arcuschin, Philip Torr, Arthur Conmy, and Neel Nanda. Understanding reasoning in thinking language models via steering vectors. *arXiv preprint arXiv:2506.18167*, 2025.
- Boshi Wang, Sewon Min, Xiang Deng, Jiaming Shen, You Wu, Luke Zettlemoyer, and Huan Sun. Towards understanding chain-of-thought prompting: An empirical study of what matters. *arXiv preprint arXiv:2212.10001*, 2022.
- Boshi Wang, Sewon Min, Xiang Deng, Jiaming Shen, You Wu, Luke Zettlemoyer, and Huan Sun. Towards understanding chain-of-thought prompting: An empirical study of what matters, 2023. URL <https://arxiv.org/abs/2212.10001>.
- Jiawei Wang, Jiakai Liu, Yuqian Fu, Yingru Li, Xintao Wang, Yuan Lin, Yu Yue, Lin Zhang, Yang Wang, and Ke Wang. Harnessing uncertainty: Entropy-modulated policy gradients for long-horizon llm agents. *arXiv preprint arXiv:2509.09265*, 2025a.
- Peiyi Wang, Lei Li, Zhihong Shao, R. X. Xu, Damai Dai, Yifei Li, Deli Chen, Y. Wu, and Zhifang Sui. Math-shepherd: Verify and reinforce llms step-by-step without human annotations, 2024. URL <https://arxiv.org/abs/2312.08935>.
- Shenzhi Wang, Le Yu, Chang Gao, Chujie Zheng, Shixuan Liu, Rui Lu, Kai Dang, Xionghui Chen, Jianxin Yang, Zhenru Zhang, et al. Beyond the 80/20 rule: High-entropy minority tokens drive effective reinforcement learning for llm reasoning. *arXiv preprint arXiv:2506.01939*, 2025b.
- Weixun Wang, Shaopan Xiong, Gengru Chen, Wei Gao, Sheng Guo, Yancheng He, Ju Huang, Jiaheng Liu, Zhendong Li, Xiaoyang Li, et al. Reinforcement learning optimization for large-scale learning: An efficient and user-friendly scaling library. *arXiv preprint arXiv:2506.06122*, 2025c.

-
- Xuezhi Wang and Denny Zhou. Chain-of-thought reasoning without prompting. In A. Globerson, L. Mackey, D. Belgrave, A. Fan, U. Paquet, J. Tomczak, and C. Zhang (eds.), *Advances in Neural Information Processing Systems*, volume 37, pp. 66383–66409. Curran Associates, Inc., 2024. URL https://proceedings.neurips.cc/paper_files/paper/2024/file/7a8e7fd295aa04eac4b470ae27f8785c-Paper-Conference.pdf.
- Ronald J Williams. Simple statistical gradient-following algorithms for connectionist reinforcement learning. *Machine learning*, 8(3):229–256, 1992.
- Yotam Wolf, Binyamin Rothberg, Dorin Shteyman, and Amnon Shashua. Compositional hardness of code in large language models – a probabilistic perspective, 2025. URL <https://arxiv.org/abs/2409.18028>.
- Guangxuan Xiao, Yuandong Tian, Beidi Chen, Song Han, and Mike Lewis. Efficient streaming language models with attention sinks. *arXiv preprint arXiv:2309.17453*, 2023.
- Huajian Xin, Z. Z. Ren, Junxiao Song, Zhihong Shao, Wanxia Zhao, Haocheng Wang, Bo Liu, Liyue Zhang, Xuan Lu, Qiushi Du, Wenjun Gao, Qihao Zhu, Dejian Yang, Zhibin Gou, Z. F. Wu, Fuli Luo, and Chong Ruan. Deepseek-prover-v1.5: Harnessing proof assistant feedback for reinforcement learning and monte-carlo tree search, 2024. URL <https://arxiv.org/abs/2408.08152>.
- An Yang, Beichen Zhang, Binyuan Hui, Bofei Gao, Bowen Yu, Chengpeng Li, Dayiheng Liu, Jianhong Tu, Jingren Zhou, Junyang Lin, et al. Qwen2. 5-math technical report: Toward mathematical expert model via self-improvement. *arXiv preprint arXiv:2409.12122*, 2024.
- An Yang, Anfeng Li, Baosong Yang, Beichen Zhang, Binyuan Hui, Bo Zheng, Bowen Yu, Chang Gao, Chengen Huang, Chenxu Lv, et al. Qwen3 technical report. *arXiv preprint arXiv:2505.09388*, 2025a.
- Sohee Yang, Elena Gribovskaya, Nora Kassner, Mor Geva, and Sebastian Riedel. Do large language models latently perform multi-hop reasoning?, 2025b. URL <https://arxiv.org/abs/2402.16837>.
- Shunyu Yao, Noah Shinn, Pedram Razavi, and Karthik Narasimhan. τ -bench: A benchmark for tool-agent-user interaction in real-world domains. *arXiv preprint arXiv:2406.12045*, 2024.
- Qiyang Yu, Zheng Zhang, Ruofei Zhu, Yufeng Yuan, Xiaochen Zuo, Yu Yue, Weinan Dai, Tiantian Fan, Gaohong Liu, Lingjun Liu, et al. Dapo: An open-source llm reinforcement learning system at scale. *arXiv preprint arXiv:2503.14476*, 2025.
- Yu Yue, Yufeng Yuan, Qiyang Yu, Xiaochen Zuo, Ruofei Zhu, Wenyuan Xu, Jiase Chen, Chengyi Wang, Tiantian Fan, Zhengyin Du, et al. Vapo: Efficient and reliable reinforcement learning for advanced reasoning tasks. *arXiv preprint arXiv:2504.05118*, 2025.
- Chujie Zheng, Shixuan Liu, Mingze Li, Xiong-Hui Chen, Bowen Yu, Chang Gao, Kai Dang, Yuqiong Liu, Rui Men, An Yang, Jingren Zhou, and Junyang Lin. Group sequence policy optimization, 2025. URL <https://arxiv.org/abs/2507.18071>.
- Zifan Zheng, Yezhaohui Wang, Yuxin Huang, Shichao Song, Mingchuan Yang, Bo Tang, Feiyu Xiong, and Zhiyu Li. Attention heads of large language models: A survey. *arXiv preprint arXiv:2409.03752*, 2024.
- Daniel M Ziegler, Nisan Stiennon, Jeffrey Wu, Tom B Brown, Alec Radford, Dario Amodei, Paul Christiano, and Geoffrey Irving. Fine-tuning language models from human preferences. *arXiv preprint arXiv:1909.08593*, 2019.

Appendix

A Experimental Details

A.1 Analysis in Sec. 4

For experimental validation, we analyze attention dynamics using **Qwen3-4B-Base** (Yang et al., 2025a) on prompts from the **GSM8K** dataset (Cobbe et al., 2021a), with sampling temperature $T = 0.7$. Each prompt is constructed by first providing the system instruction: System: Please reason step by step, and put your final answer within `\boxed{\}`. We then decompose the problem into a Context and a Question field, as illustrated in Prompt A.1.

We first generate a response using standard autoregressive decoding. Once the full response is obtained, we concatenate it with the original prompt and perform a *single additional forward pass* through the model-using an eager attention implementation-to extract the full attention maps via the Hugging Face `transformers` library. From this, we isolate the attention patterns corresponding to the response tokens for analysis.

In computing the Windowed Attention Activation Density (WAAD), we set the temporal window size to $W = 10$, as we are primarily interested in local attention dependencies. For the Forward Attention Influence (FAI) metric, we define the influence scope to span from each token position to the end of the response.

Our analysis comprises two components: (i) For quantification analysis (e.g., Tables 1 and 2), we randomly sample 70 GSM8K problems and examine the relationship between attention-based metrics across all generated tokens; (ii) For qualitative analysis (e.g., Fig. 2), we select the problem with the shortest correct response to facilitate clear and interpretable plots. The full prompt and model response for this example are provided below:

Input Prompt

System: Please reason step by step, and put your final answer within `\boxed{\}`.
Context: Siobhan has 2 fewer jewels than Aaron. Aaron has 5 more jewels than half of Raymond’s jewels.
Question: If Raymond has 40 jewels, how many jewels does Siobhan have?

The response for analysis is:

Response

Step 1: Determine how many jewels Aaron has. Aaron has 5 more jewels than half of Raymond’s jewels. Raymond has 40 jewels. Half of Raymond’s jewels = $40 / 2 = 20$. So, Aaron has $20 + 5 = 25$ jewels.
Step 2: Determine how many jewels Siobhan has. Siobhan has 2 fewer jewels than Aaron. So, Siobhan has $25 - 2 = 23$ jewels.
Final answer: Siobhan has 23 jewels.

Experimental Details of Table 2. Table 2 reports correlation analyses between the attention-based metrics visualized in Fig. 2. The specific protocols for computing these correlations are as follows:

- **Average Entropy of the WAAD Peaks:** We compute the average entropy at token positions identified as WAAD peaks (reported as “observed”) and compare it against the average entropy over all response tokens (reported as “random”). A higher observed value indicates that WAAD peaks correspond to positions of significantly greater uncertainty.
- **Receiver & Global FAI Peak Co-occurrence:** We measure the alignment between peaks identified by receiver-head FAI (Bogdan et al., 2025) and those identified by global-head FAI. Specifically, we report the fraction of receiver FAI peaks that overlap with global FAI peaks (reported as “observed”). The “random” baseline denotes the expected overlap if receiver FAI peaks were uniformly distributed across all response positions, i.e., the proportion of Global FAI peaks among all tokens. An increase over this baseline signifies strong structural correspondence between the two FAI variants.
- **FAI Follows/Coincides with WAAD Peak:** We evaluate the extent to which FAI peaks coincide with or immediately follow WAAD peaks. The “observed” value is the proportion of FAI

peaks satisfying this temporal condition relative to all FAI peaks. The “random” baseline is the expectation by randomly shuffling FAI peak positions (preserving their count) and recomputing the overlap. A higher observed value demonstrates non-random alignment between attention activation density and forward influence.

A.2 RL Experiments in Sec. 5

Dataset. For *Countdown*, we follow the data construction protocol of Pan et al. (2025) and use a test set of 512 instances (each containing four input numbers), along with a training set of 20,000 samples. The *CrossThink-QA* dataset is sourced from Akter et al. (2025). For mathematical reasoning tasks, models are trained on DAPO-Math-17K (Yu et al., 2025).

Benchmark Details. We evaluate our method across a spectrum of reasoning tasks, ranging from relatively simple puzzles and general question-answering (QA) to challenging mathematical reasoning benchmarks. Specifically, our evaluation suite includes:

- *Countdown* (Pan et al., 2025): A symbolic reasoning puzzle in which the model is given four integers and must construct a valid arithmetic expression using basic operations (+, −, ×, ÷) to reach a specified target number. This task tests compositional planning and precise execution under constraints.
- *CrossThink-QA* (Akter et al., 2025): A diverse, multi-domain QA dataset that aggregates questions from heterogeneous sources (e.g., science, commonsense, and trivia), designed to assess general-purpose reasoning and knowledge integration across domains.
- *Mathematical Reasoning Benchmarks*: Five established datasets spanning a wide range of difficulty and problem types:
 - **AIME24** and **AIME25**: Collections of problems from the American Invitational Mathematics Examination (2024 and 2025) ¹, featuring non-routine problems requiring multi-step insight.
 - **AMC** (Li et al., 2024): Problems from the American Mathematics Competitions, emphasizing logical deduction and problem-solving under time constraints.
 - **MATH500** (Hendrycks et al., 2021): A set of 500 challenging problems from the MATH dataset, covering algebra, geometry, number theory, and combinatorics.
 - **OlympiadBench** (He et al., 2024): A recent collection of international mathematical olympiad-level problems, representing the frontier of machine reasoning in mathematics.

This diverse set of tasks enables us to assess both the generalizability and the depth of our method across reasoning modalities and complexity levels.

Plot Setup. The performance curves are smoothed via an Exponential Moving Average (EMA): $EMA_t = \alpha \cdot \max(x_t, EMA_{t-1}) + (1 - \alpha) \cdot EMA_{t-1}$, which reflects a running average of peak performance. When the best performance is continually updated, the curve keeps rising; if performance stalls, the curve stays flat. The curve’s endpoint therefore represents a relatively stable peak performance.

B Supplementary Results

B.1 Representative Perturbation Examples

We present illustrative cases where token perturbations at high-FAI versus low-FAI positions lead to qualitatively different reasoning behaviors. All examples use the same input prompt:

Input Prompt

System: Please reason step by step, and put your final answer within `\boxed{\}`.
Context: Terry eats 2 yogurts a day. They are currently on sale at 4 yogurts for \$5.00.
Question: How much does he spend on yogurt over 30 days?

The original response by greedy decoding is:

¹<https://maa.org/>

Original Response

To determine how much Terry spends on yogurt over 30 days, we need to follow these steps:

1. **Calculate the number of yogurts Terry eats in 30 days:** Terry eats 2 yogurts per day. Therefore, in 30 days, he will eat:

$$2 \text{ yogurts/day} \times 30 \text{ days} = 60 \text{ yogurts}$$

2. **Determine the cost per yogurt:**

The yogurts are on sale at 4 yogurts for \$5.00. To find the cost per yogurt, we divide the total cost by the number of yogurts:

$$\frac{5.00 \text{ dollars}}{4 \text{ yogurts}} = 1.25 \text{ dollars/yogurt}$$

3. **Calculate the total cost for 60 yogurts:** Now, we multiply the cost per yogurt by the total number of yogurts Terry will eat in 30 days:

$$60 \text{ yogurts} \times 1.25 \text{ dollars/yogurt} = 75.00 \text{ dollars}$$

Therefore, Terry spends 75.00 dollars on yogurt over 30 days.

We now perform perturbations at high-FAI positions, selecting other tokens from the top-k candidates and rolling out continuations to observe how the subsequent reasoning trajectory changes.

High-FAI Example 1: Perturbation at “much” (Position 4 in response)

Original token: much

Perturbed token: many

Jaccard similarity: 0.383

Perturbed continuation:

To determine how many yogurts Terry will eat in 30 days, we start by calculating the total number of yogurts he consumes:

$$\text{Total} = 2 \text{ yogurts/day} \times 30 \text{ days} = 60 \text{ yogurts}$$

Next, we need to figure out how many sets of 4 yogurts he can buy with his 60 yogurts. Since the yogurts are on sale at 4 for \$5.00, we divide the total number of yogurts by 4:

$$\text{Sets of 4 yogurts} = \frac{60 \text{ yogurts}}{4 \text{ yogurts/set}} = 15 \text{ sets}$$

Now, we calculate the total cost by multiplying the number of sets by the cost per set:

$$\text{Total cost} = 15 \text{ sets} \times \$5.00/\text{set} = \$75.00$$

Therefore, Terry spends 75 dollars on yogurt over 30 days.

In the example above, we observe a notable shift in the reasoning logic. Structurally, the response skips the initial planning phase and jumps directly into computation, abandoning the original plan-then-solve format. Moreover, the computational approach itself differs substantially. For instance, by framing the problem in terms of sets of yogurts rather than per-unit cost. Despite these changes, the final answer remains correct. Nevertheless, when compared to the original response, the content-word overlap at the token level is only 0.383, indicating significant divergence in the reasoning trajectory. We observe that sometimes the change to the token may appear minor, yet the model still frequently attends back to this position internally. Thus, even when the surface semantics seem alike, it can exert a disproportionately large influence on subsequent reasoning.

High-FAI Example 2: Perturbation at “much” (Position 4 in response)

Original token: much

Perturbed token: long

Jaccard similarity: 0.255

Perturbed continuation:

To determine how long Terry will be able to eat yogurt for \$50, we need to calculate how many yogurts he can buy with that amount of money and then figure out how many days that will last. First, let’s find out how many yogurts Terry can buy with \$50. Since the yogurts are on sale at 4 for \$5.00, we can calculate the cost per yogurt as follows:

Cost per yogurt = \$5.00 / 4 yogurts = \$1.25 per yogurt

Now, let’s calculate how many yogurts Terry can buy with \$50:

Number of yogurts = \$50 / \$1.25 per yogurt = 40 yogurts

Since Terry eats 2 yogurts a day, we can now calculate how many days he can eat yogurt for:

Number of days = 40 yogurts / 2 yogurts per day = 20 days

Therefore, Terry will be able to eat yogurt for 20 days with \$50.

In this example, when we replace the token at the same position with the third-highest-probability candidate, we observe that the model’s reasoning completely deviates from the correct path, leading to an incorrect final answer. When compared to the original response, the content-word overlap at the token level is only 0.255, indicating significant divergence in the reasoning trajectory.

Next, we examine the effects of perturbing low-FAI tokens by comparing the resulting reasoning trajectories after substitution. This allows us to assess how changes to less influential tokens impact the model’s subsequent reasoning.

Low-FAI Example 1: Perturbation at “over” (Position 9 in response)

Original token: over

Perturbed token: in

Jaccard similarity: 1.000

Perturbed continuation:

To determine how much Terry spends on yogurt in 30 days, we need to follow these steps:

1. ****Calculate the number of yogurts Terry eats in 30 days:**** Terry eats 2 yogurts per day. Therefore, in 30 days, he will eat:

$$2 \text{ yogurts/day} \times 30 \text{ days} = 60 \text{ yogurts}$$

2. ****Determine the cost per yogurt:**** The yogurts are on sale at 4 yogurts for \$5.00. To find the cost per yogurt, we divide the total cost by the number of yogurts:

$$\frac{5.00 \text{ dollars}}{4 \text{ yogurts}} = 1.25 \text{ dollars/yogurt}$$

3. ****Calculate the total cost for 60 yogurts:**** Now, we multiply the cost per yogurt by the total number of yogurts Terry will eat in 30 days:

$$60 \text{ yogurts} \times 1.25 \text{ dollars/yogurt} = 75.00 \text{ dollars}$$

Therefore, Terry spends 75.00 dollars on yogurt over 30 days.

In this case, we observe a particularly interesting phenomenon: when replacing the token “over” in “over 30 days” with “in”, the only change occurs at that specific position, and the subsequent reasoning trajectory remains completely unchanged. The Jaccard similarity between the perturbed and original outputs is 1.00, indicating identical content-word sets. This suggests that the choice of token at this position is governed purely by local syntactic or stylistic preferences and exerts no influence on the global reasoning process.

Low-FAI Example 2: Perturbation at “spends” (Position 6 in response)

Original token: spends

Perturbed token: will

Jaccard similarity: 0.946

Perturbed continuation:

To determine how much Terry will spend on yogurt over 30 days, we need to follow these steps:

1. **Calculate the number of yogurts Terry eats in 30 days:** Terry eats 2 yogurts per day. Therefore, in 30 days, he will eat:

$$2 \text{ yogurts/day} \times 30 \text{ days} = 60 \text{ yogurts}$$

2. **Determine the cost per yogurt:** The yogurts are on sale at 4 yogurts for \$5.00. To find the cost per yogurt, we divide the total cost by the number of yogurts:

$$\frac{5.00 \text{ dollars}}{4 \text{ yogurts}} = 1.25 \text{ dollars/yogurt}$$

3. **Calculate the total cost for 60 yogurts:** Now, we multiply the cost per yogurt by the total number of yogurts Terry will eat:

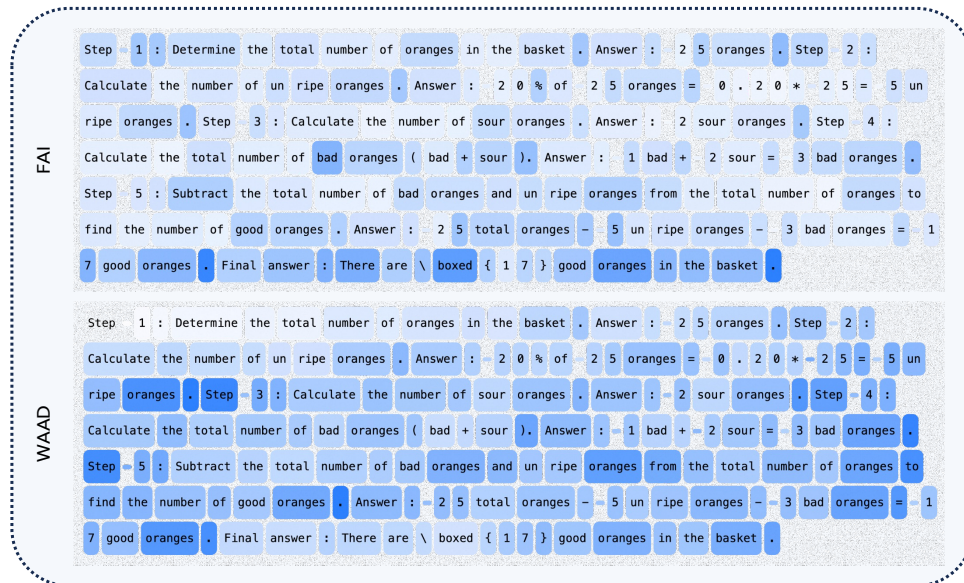
$$60 \text{ yogurts} \times 1.25 \text{ dollars/yogurt} = 75.00 \text{ dollars}$$

Therefore, Terry will spend 75.00 dollars on yogurt over 30 days.

The example above exhibits the same pattern: the token replacement affects only the local phrasing, while the overall reasoning logic remains essentially unchanged. The model follows the same solution strategy, performs identical calculations, and arrives at the same final answer, confirming that such low-FAI tokens typically serve a surface-level role without altering the core inference trajectory.

B.2 Visualization of FAI and WAAD Distributions on Tokens

We visualize the token-level distributions of FAI and WAAD by directly outputting responses to randomly sampled math problems from GSM8K, computing FAI and WAAD for each token, and encoding their magnitudes via color intensity. As shown in Fig 8, tokens with high FAI typically retain intermediate reasoning results, while tokens with high WAAD often mark the beginning of a new reasoning chunk for the model. We also observe that punctuation tokens, such as commas, periods, and line breaks, consistently attract elevated attention weights across multiple layers and heads. We hypothesize that this phenomenon arises because punctuation marks appear periodically in the generated text and serve as natural syntactic and semantic boundaries. The attention mechanism, being sensitive to such regular structural cues, tends to form recurrent connections between these tokens. Thus, at these points, the model consolidates contextual evidence from preceding tokens and redistributes summarized signals to guide subsequent reasoning steps.



Case 1



Case 2

Figure 8: Visualization cases of the token-level distributions of FAI and WAAD.